Materials Science in Semiconductor Processing 39 (2015) 30–39

Contents lists available at ScienceDirect

Materials Science in Semiconductor Processing

journal homepage: www.elsevier.com/locate/mssp

Structure and characteristics of reactive magnetron sputtered (CrTaTiVZr)N coatings

Zue-Chin Chang [a,*], Du-Cheng Tsai [b], Erh-Chiang Chen [b]

[a] Department of Mechanical Engineering, National Chin-Yi University of Technology, Taichung 411, Taiwan
[b] Department of Materials Science and Engineering, National Chung Hsing University, Taichung 40227, Taiwan

ARTICLE INFO

Available online 14 May 2015

Keywords:
Multi-element nitride
Structure
XRD
TEM

ABSTRACT

$(CrTaTiVZr)N_x$ coatings were deposited via reactive radio frequency magnetron sputtering. We investigated the effects of substrate bias at 0 V to −200 V on the chemical composition, microstructure, as well as mechanical and electrical properties of the coatings. All these coatings have a single NaCl-type face-centered cubic structure. The increase of substrate bias results in the transformation of preferred orientation from (111) to (200) out-of-plane. At the substrate bias of 0 V, the deposited coatings are composed of V-shaped columnar grains with void boundaries and faceted surfaces, which contribute to the tensile stress in the deposited coatings. The grain refinement and lattice expansion increase gradually with increasing substrate bias up to −100 V. A typical columnar structure converts into a dense and featureless structure. Further increase of substrate bias results in the decrease of lattice parameter, which may be due to stress relaxation. The internal stress in the deposited coatings is also strongly dependent on the substrate bias. The increase of substrate bias results in the transition of tensile to compressive stress and increase of compressive stress in the deposited coatings. Accordingly, the physical properties are improved significantly by applying moderate substrate bias. At the optimized substrate bias of −100 V, the high hardness value of 36.4 GPa, low electrical resistivity of 131 μΩ-cm, and high light reflectivity near 2000 nm of 74% are achieved.

1. Introduction

Since the 1970s, a novel alloy system called high-entropy alloys (HEAs), which are composed of at least five principal elements and with concentrations between 5 at% and 35 at%, has been developed rapidly. Because of four core effects, namely, high mixing entropy, lattice distortion, sluggish diffusion, and cocktail effect, the HEAs have been found to develop simple solid solution structures and versatile properties, such as high cast hardness, good thermal stability, and corrosion resistance; thus, they have gained significant attention for their potential use in various applications [1–4]. Based on the design concept of HEAs, HEA coatings made of metals, oxides, carbides, and nitrides are also investigated intensively and are shown to have high potential for coating application.

Reactive magnetron sputtering has been widely used in producing numerous types of HEA nitride coatings. HEA nitride coatings such as (TiZrNbHfTa)N [5], (AlCrTaTiZr)N [6], (AlCrMoTaTi)N [7,8], (AlCrTiVZr)N [9], (CrHfTiVZr)N [10], (AlCrSiTiZr)N [11], and (AlMoNbSiTaTiVZr)N [12] have been found to have high mechanical properties, which indicate high potential as protective coatings. The significant influences of the nitrogen flow, target power, substrate temperature, and bias on the structure and properties of the HEA nitride films have been confirmed by previous studies. So far, most research focusses on the mechanical properties of the HEA nitride

* Corresponding author. Tel.: +886 4 2392 4505; fax: +886 4 2293 0681.
E-mail address: changcy7188@gmail.com (Z.-C. Chang).

http://dx.doi.org/10.1016/j.mssp.2015.04.045
1369-8001/

coatings. Other properties are usually ignored and therefore limits their development in various types of application. It is expected that HEA nitrides could be multifunctional coatings. For example, TiN, ZrN, TaN have attracted interest for applications in semiconductor device such as diffusion barriers [13–15]. TiN and ZrN coatings are also expected to be a candidate for a high IR reflector [16,17]. VN shows a generation of surface layer acting as solid lubricant due to its oxidation [18]. CrN is considered to be competent for high speed machining of the hardworking materials [19]. As a result of the combination of these individual nitrides with different functionality, HEA nitride may have wide application potential. Therefore, we study the mechanical and electro-optical properties of (CrTaTiVZr)N coatings. On the other hand, HEA nitrides are well known to have a columnar structure with FCC [NaCl-type] phase. These studies proved that negative substrate bias voltage is an important process parameter to tailor the morphology, structure, and mechanical properties of HEA nitride coatings. However, the growth mechanism of structural evolution of HEA nitrides was seldom reported. Primary resultant coating properties in this study include residual stress, lattice parameter, grain size, and microstructure. An attempt is made to propose a detailed describing the growth mechanism of unbiased and biased (CrTaTiVZr)N coatings. Thus, in this study, (CrTaTiVZr)N coatings were deposited at six different bias voltages, while other deposition parameters were kept constant. The structure as well as mechanical and electro-optical properties of the nitride coatings were subsequently characterized.

2. Experimental

The (CrTaTiVZr)N coatings were deposited on Si (100) wafers by an RF magnetron sputtering system using equimolar CrTaTiVZr targets 75 mm in diameter. The target alloy was fabricated by conventional powder metallurgy technology. Before deposition, the Si substrates were cleaned and rinsed with ethanol and distilled water in an ultrasonic bath. The sputtering chamber was pumped down to 2.67×10^{-4} Pa using a turbo pump. The deposition of the (CrTaTiVZr)N coatings was carried out in an $Ar+N_2$ mixed atmosphere under a RF power of 350 W and a working pressure of 6.67×10^{-1} Pa. During deposition, the Ar and N_2 flow rates are 100 and 4 SCCM, respectively. The substrate bias was chosen as the controlling parameter, which varied from 0 to −200 V. The distance between the substrate and target was 90 mm. The deposition time was set to 60 min. The substrate temperature was fixed at 450 °C during the deposition process. The targets were presputtered by Ar to remove their surface oxide layers before deposition.

The chemical compositions of the (CrTaTiVZr)N coatings were determined by field-emission electron probe micro-analyses (FE-EPMA JOEL JXA-8800M). At least three tests were performed for each sample. The depth profiling analyses of elemental distributions of (CrTaTiVZr)N coatings were performed by secondary ion mass spectrometry (SIMS, ION-TOF TOF.SIMS IV). The crystal structures were analyzed by a glancing-incidence (1°) X-ray diffractometer (GIXRD, BRUKER D8 Discover) using Cu Kα radiation at a scanning speed of 1°/min. The scanning step was 0.02° and the scanning range was 20–80°. The morphology studies and thickness measurements were carried out using field emission scanning electron microscopy (SEM, JEOL JSM-6700F). The deposition rate was obtained by dividing the thickness with the deposition time. Microstructural examinations were conducted by an analytical transmission electron microscope (TEM, JEM-2100F). The residual stress of the deposited films was obtained by acquiring GIXRD patterns at various tilting angles ψ, or acquiring offset scans and plotting the d-space values versus $\cos2\alpha\ \sin2\psi$ technique, where $\alpha=\theta-\omega$ [20]. The microhardness and elastic modulus of the coatings were measured under a load of 5000 μN using a TriboLab nanoindenter (Hysitron). A Berkovich diamond indenter tip indenter was used to reduce the influence of the substrate on the microhardness and elastic modulus of the coatings. At least five tests were performed for each sample. Reflectivity was measured using a spectrophotometer (Shimadzu UV-3600).

3. Results

The concentrations of all elements in the (CrTaTiVZr)N coatings deposited at various substrate biases are presented in Fig. 1. The concentration of all target elements is almost unaffected by substrate bias. A slight decrease of nitrogen content with increasing substrate bias, which suggests more energetic ion bombardment at a larger substrate bias, could allow nitrogen atoms in disequilibrium sites to escape from the surface.

The XRD patterns of the (CrTaTiVZr)N coatings are greatly affected by the substrate bias. Fig. 2 shows the XRD patterns for as-deposited (CrTaTiVZr)N coatings deposited at the substrate bias of 0, −25, −50, −100, −150, and −200 V. The (200), (220), and (311) peaks of the (CrTaTiVZr)N coatings are indexed as belonging to an FCC structure of the B1 phase (NaCl-type). As Fig. 2 shows, the increase of substrate bias results in the shift and broadening of all XRD diffraction peaks.

To better observe the influence of the substrate bias on the diffraction intensity and full width at half maximum (FWHM) of the different peaks, the XRD patterns are fitted using a mixture of Gaussian and Lorentzian profiles. Further, from the FWHA, the average grain size of the films was calculated using Scherrer's formula [21]. The influence of the substrate bias on the grain size is

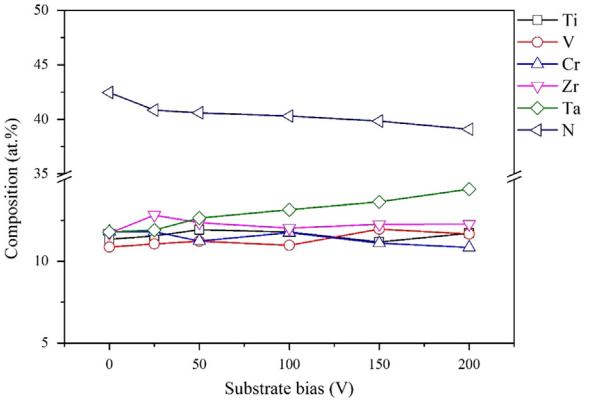

Fig. 1. EPMA element contents in (CrTaTiVZr)N coatings deposited at different substrate biases.

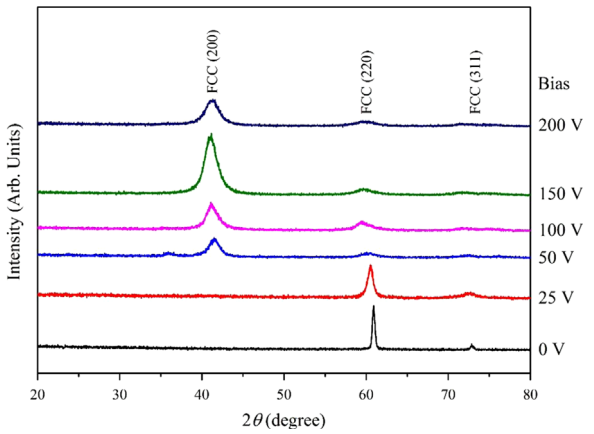

Fig. 2. X-ray diffraction pattern of the (CrTaTiVZr)N coatings deposited at different substrate biases.

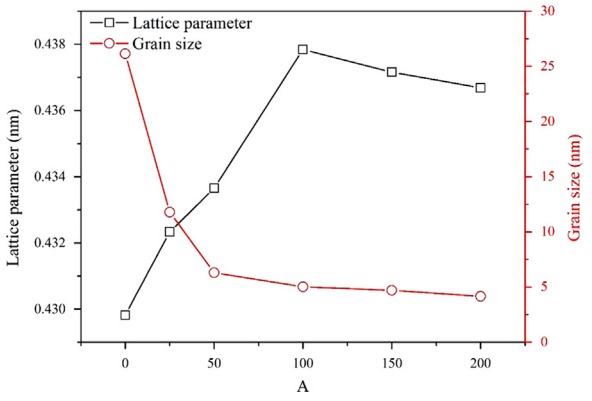

Fig. 3. Lattice parameter and average grain size of the (CrTaTiVZr)N coatings deposited at different substrate biases.

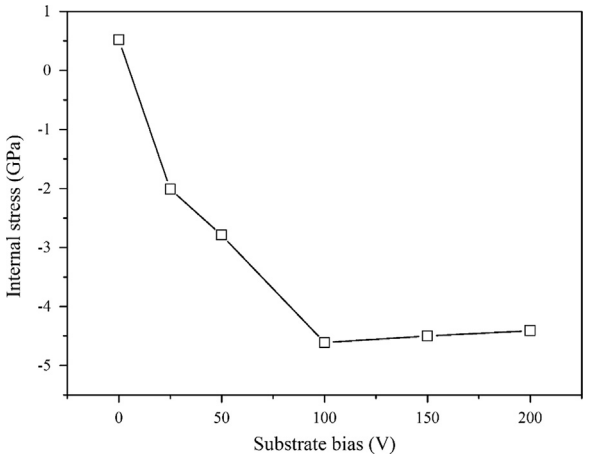

Fig. 4. Internal stress of the (CrTaTiVZr)N coatings deposited at different substrate biases.

illustrated in Fig. 3. The grain size shows a marked decrease with substrate bias increases from 0 to −50 V. Thereafter, increases in the bias result in the slight decrease of the grain size.

A shift of XRD peaks to lower angles is observed with increasing substrate bias. This result indicates an increase in the lattice parameters of the (CrTaTiVZr)N coatings, as shown in Fig. 3. The lattice parameters for the deposited (CrTaTiVZr)N coatings increase gradually from 0.4298 nm with increasing substrate bias from 0 V and reach the maximum of 0.4378 nm at the bias of −100 V. Then, a further increase of substrate bias results in a slight decrease of the lattice parameter to 0.4367 nm for the deposited coatings. The influence of internal stress in the deposited (CrTaTiVZr)N coatings on the calculated crystallite size and lattice parameters is not considered in the present analysis because they have a similar variation trend with substrate bias. The internal stress in the (CrTaTiVZr)N coatings is plotted in Fig. 4 as a function of substrate bias. For the coatings deposited at the substrate bias of 0 V, the internal stress is slightly tensile at 0.52 GPa. With the increase of substrate bias to −25 V, a tensile to compressive stress transition can be observed. As the substrate bias increases to −100 V, a maximum compressive stress of −4.61 GPa was obtained. Thereafter, further increasing substrate bias results in a slight decrease of the compressive stress. This kind of tensile–compressive stress transition as a function of the substrate bias has also been observed by Shen et al. in $(Al_{1.5}CrNb_{0.5}Si_{0.5}Ti)N_x$ coating prepared by using direct current sputtering [22].

The preferred orientation of the films could be quantified by evaluating integrated intensities of four apparent peaks, namely, (111), (200), (220), and (311). The intensity of the preferred orientation is defined using the following equation:

$$\text{Texture coefficient} = \frac{I_{hkl}/I^0_{hkl}}{\left(\frac{1}{n}\right)\sum_0^n I_{hkl}/I^0_{hkl}}$$

where I_{hkl} is the measured peak integrated intensity of the (hkl) [(hkl)=(200), (220), or (220)] plane, n is the number of diffraction reflections. I^0_{hkl} is the reference standard (random) peak intensity for the reflection (hkl), JCPDS values of peak intensity were used. The random oriented XRD patterns of the (CrTaTiVZr)N is unknown, but could be approximated from bulk binary nitride using the mixture rule. A change in the preferred orientation is observed with the increase of substrate bias, as shown in Fig. 5. This texture coefficient of coatings is clearly changed from the (220) plane to the (200) plane with increasing substrate bias. The influence of substrate bias on preferred orientation has been investigated frequently. Some previous studies reported that the preferred orientation of thin films with a NaCl-type structure was determined by the competition between surface energy and strain energy. For a NaCl-type crystal structure, the (111) plane had the lowest strain energy while the (200) plane had the lowest surface energy. The strain energy consideration favored the growth of (111) orientation especially for film deposited at high substrate bias [23]. By further increasing substrate bias, the (220) preferred orientation is expected because of ion channeling and lower energy loss in this more open direction over a long distance [24,25]. For example, Lee et al. [26] and Kobayashi and Doi [27] observed a change from (002) into (111) and then into (220) with increasing bias voltage. Similarly, Pastalas et al. [28] and Khan et al. [29] reported a change from (002) to (111). Other studies reported that preferred orientation changed

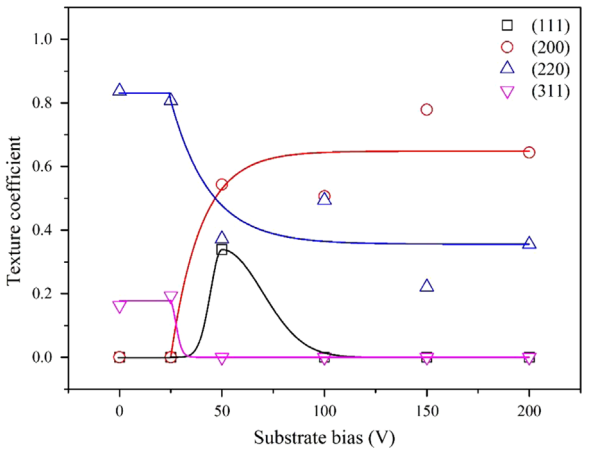

Fig. 5. Texture coefficient of the (CrTaTiVZr)N coatings deposited at different substrate biases.

from (002) to (111) and then to (002) with increasing bias voltage [24,25]. They demonstrate that the (220) preferred orientation is formed only under very high bias voltage conditions, which is not consistent with the findings of the present study. The unusual phenomenon may be attributed to the difference of analysis method. In this study, the crystal structure was analyzed by a glancing-incidence (1°) XRD (GIXRD) instrument and this orientation of the observed crystal is not parallel to the surface. Although this variation trend of the observed preferred orientation is usually similar to that of out-of-plane (parallel to substrate normal) orientation, the deviation may occur for coating with an extremely high degree of out-of-plane orientation. The subsequent cross-sectional TEM analysis can provide more accurate information.

Fig. 6 represents typical SEM micrographs for the coatings deposited at various substrate biases. The coatings without substrate bias show a clear columnar surface with a faceted surface. With increasing substrate bias to −50 V, the coating displays a more compact and less defined columnar structure. The coating with a substrate of −100 V and above appears to have an extremely fine structure with a smooth surface. However, the structure evolution cannot be identified completely by SEM. Thus, a further TEM observation was used in the comprehensive characterization of structure evolution. Fig. 7 shows the TEM micrographs with the selected area diffraction (SAD) patterns of the (CrTaTiVZr)N coatings without substrate bias. At the initial growth stage, a continuous amorphous layer with the mazy contrast is formed. The randomly oriented nucleation occurred in the continuous amorphous layer at its initial stage. Then, the grains grew and developed a V-shaped columnar structure with the FCC (111) out-of-plane preferred orientation along coating thickness. Notably, a number of microvoids visible between the columns were formed. When substrate bias was applied to −100 V (Fig. 8), the microstructure was transformed into a fine fiber structure with dense boundaries and the out-of-plane preferred orientation was changed to (200). As for the aforementioned phenomenon, the effect of substrate bias includes (i) grain refinement, (ii) lattice expansion, (iii) (200) preferred orientation, (iv) increment of compressive stress, and (v) densification of structure.

Fig. 9 shows the hardness and elastic modulus of the as-deposited (CrTaTiVZr)N coatings deposited at different substrate biases. The hardness and elastic modulus of the as-deposited films increased from 11.3 GPa to 36.4 GPa and from 200.3 GPa to 273.8 GPa, respectively, as the substrate bias was increased from 0 to −100 V. A minimal fluctuation was observed upon further increase of the substrate bias to −200 V. The contribution can be ascribed to grain refinement, increment of compressive stress, and densification of structure. The overall hardness can be expressed by the following equation:

$$H_{total} = H_i + \Delta H_s + \Delta H_g + \Delta H_v$$

where H_i is the internal stress without stress hardening, ΔH_s is the stress hardening, ΔH_g is the grain size strengthening, and ΔH_v is the void softening. The H_i could be approximately calculated from the bulk binary nitride hardnesses by the mixture rule (CrN, ~10.8 GPa; TaN, ~14.4 GPa; TiN, ~19.9 GPa; VN, ~13.0 GPa; ZrN, ~15.0 GPa), along with the EPMA-determined composition. The multiplying factor of ΔH_s on compressive stress and tensile stress is set as 1.0 and −1.0 for simplicity, respectively. Thus, the ΔH_s is obtained directly from the abovementioned stress value in Fig. 4. The ΔH_v is also considered to be a significant factor at a substrate bias below −100 V since the visible voids along the boundaries are observed. When the substrate bias increases above −100 V, the ΔH_v is negligible since the visible voids along the boundaries disappear. The ΔH_g can be estimated using the Hall–Petch equation [30] and is expressed by the following equation:

$$\Delta H_g = H_{total} - H_i - \Delta H_v - \Delta H_s = Kd^{-1/2}$$

where K is the fitting parameter and d (nm) is the grain size. Based on above hypothesis, the ΔH_g at a substrate bias above −100 V is obtained. The K is also calculated to be around 36.23 ± 1.53 GPa nm$^{-1/2}$. With this equation, the ΔH_g and ΔH_v could be calculated for the coating deposited at a substrate bias below −100 V. Based on the preceding discussion, the effect on the hardening mechanism is summarized in Table 1. Although the aforementioned quantitative method is inaccurate, the qualitative exploration of the hardening mechanism is believed to be convincing.

Fig. 10 shows the electrical resistivity of the (CrTaTiVZr)N coatings deposited at different substrate biases. The electrical resistivity of coating without substrate bias is 446 μΩ-cm and it decreases to heavily 131 μΩ-cm, increasing the substrate bias up to −100 V. Beyond this substrate bias, the electrical resistivity of the coatings reveal a slight increase from 131 to 152 μΩ-cm. Obviously, at a substrate bias of −100 V, the decrease of void scattering and grain size dominates the decreasing trend of the electrical resistivity. By further increasing the substrate bias, the grain boundary scattering becomes important because of the extremely small grain size and the void elimination becomes limited. The slight increased electrical resistivity is attributed to the higher grain boundary scattering.

Fig. 11 shows the light reflectivity of the (CrTaTiVZr)N coating at wavelengths varying from 300 nm to 2400 nm was measured at room temperature. All the coatings

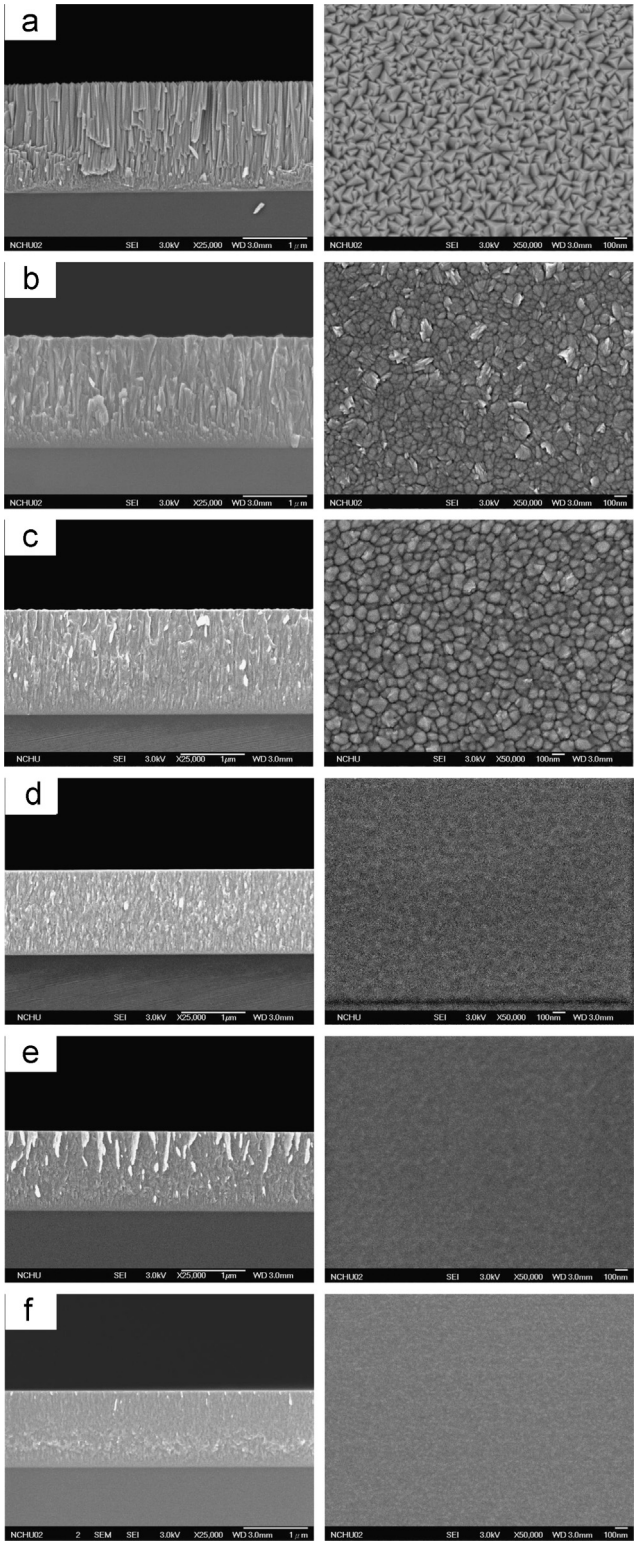

Fig. 6. SEM micrographs of the (CrTaTiVZr)N coatings deposited at different substrate biases: (a) 0 V, (b) −25 V, (c) −50 V, (d) −100 V, (e) −150 V, and (f) −200 V.

exhibit a low reflectivity in the short wavelength range from 300 to 700 nm. As the wavelength increases, the reflectivity exhibits a sharp increase and then reaches a high reflectivity. The behavior can be viewed as the characteristics of a free-electron metal as described by the Drude model [31,32]. Moreover, the light reflectivity of

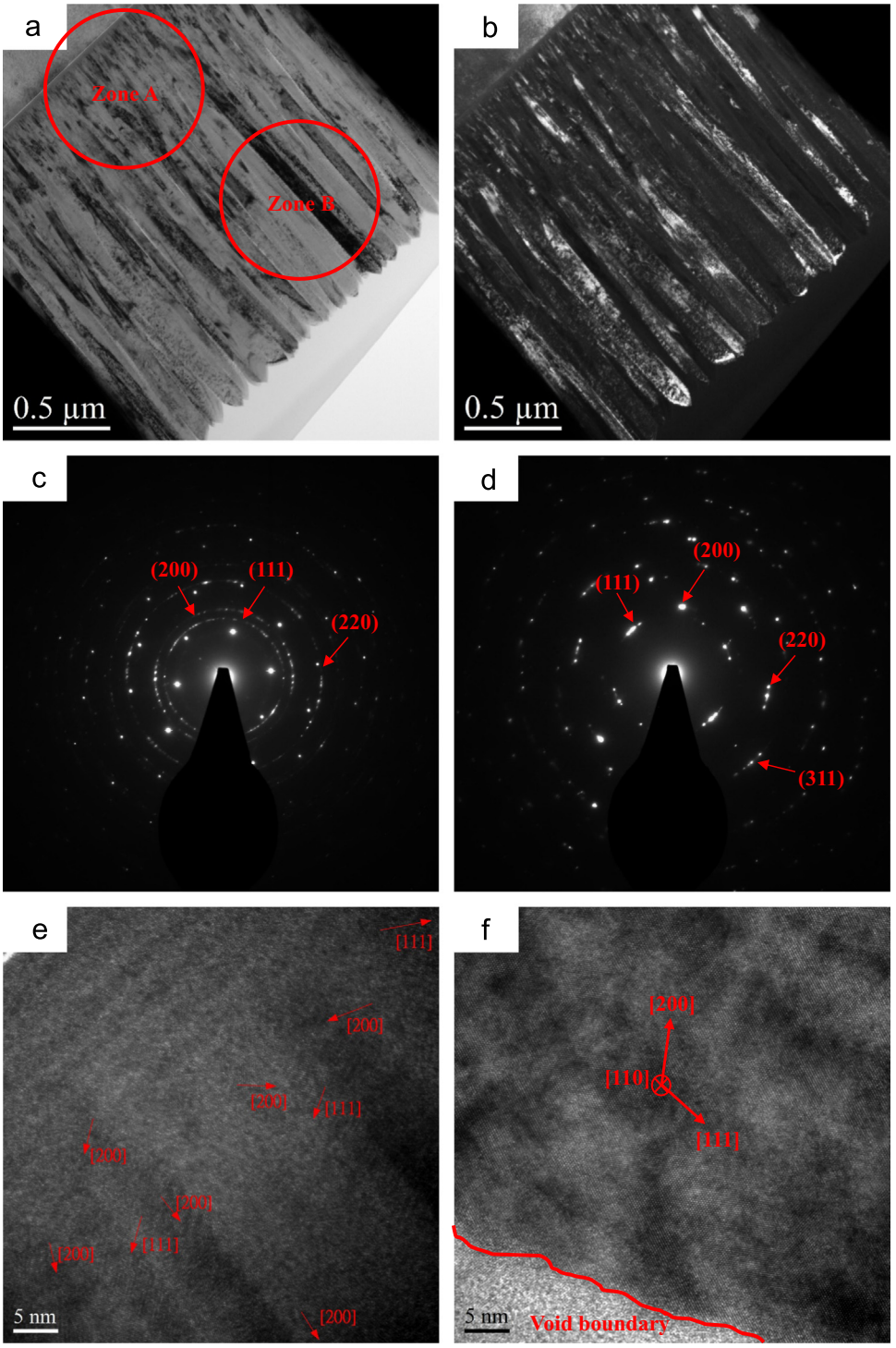

Fig. 7. Cross-sectional TEM micrographs of the (CrTaTiVZr)N coatings without substrate bias. (a) Bright-field image. (b) Dark-field image using the (111) and (200) diffraction rings. (c) SAD patterns of Zone A of the cross-section. (d) SAD patterns of top part of Zone B of the cross-section. (e) High resolution TEM lattice image of bottom part of the cross-section. (f) High resolution TEM lattice image of top part of the cross-section.

coating without substrate bias is about 53% near 2000 nm. As the substrate bias increases to −100 V, the light reflectivity near 2000 nm reach maximum values of 74%. Then, further increase of substrate bias leads to a slight decrease of light reflectivity. It has been reported that the magnitude of the light reflectivity is determined by the roughness of the surfaces, grain size, the amount of voids, and also the content of impurities [33]. Because the coatings are more densified with the application of substrate biases, the light reflectivity is accordingly improved.

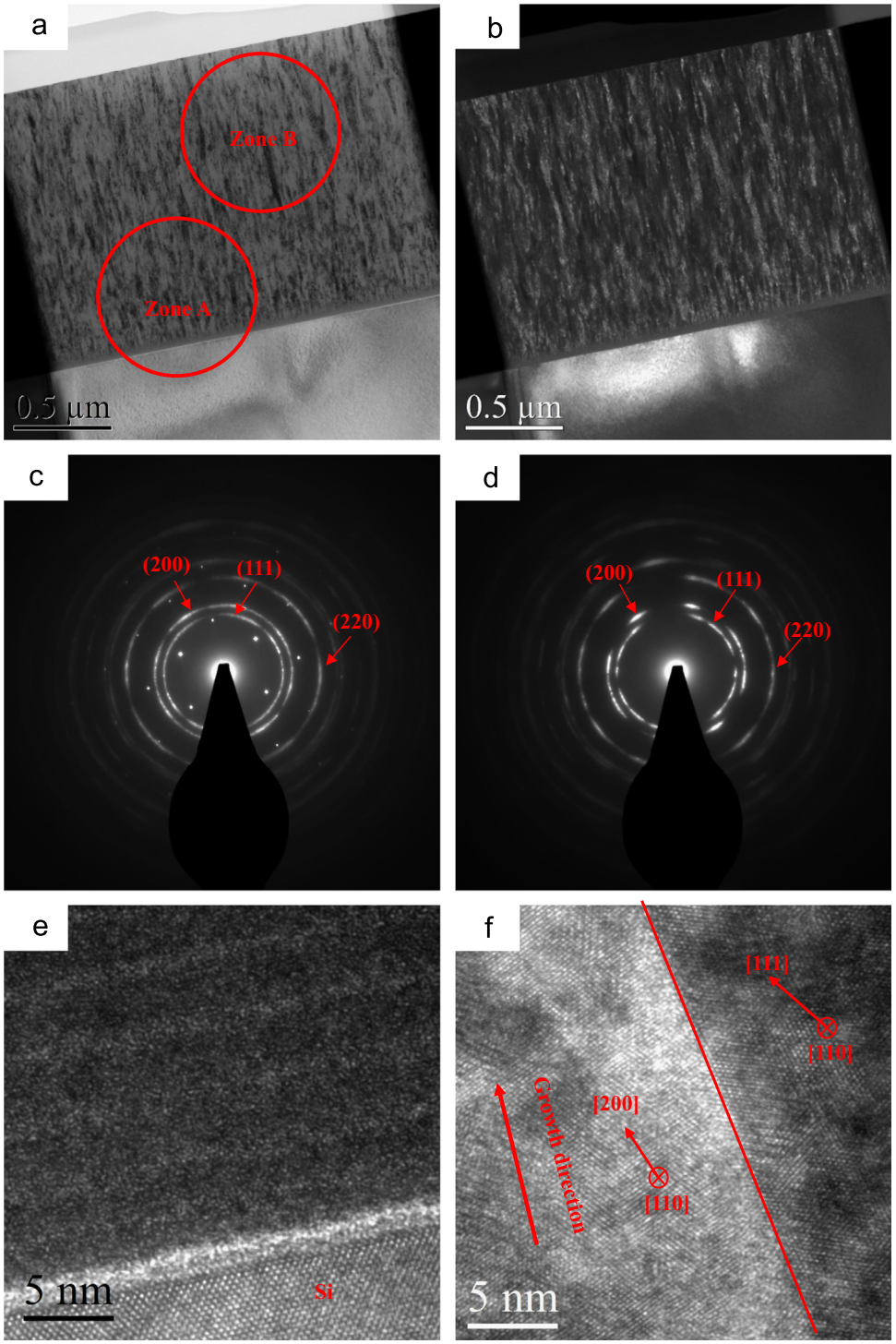

Fig. 8. Cross-sectional TEM micrographs of the (CrTaTiVZr)N coatings deposited at substrate bias of −100 V. (a) Bright-field image. (b) Dark-field image using the (111) and (200) diffraction rings. (c) SAD patterns of Zone A of the cross-section. (d) SAD patterns of top part of Zone B of the cross-section. (e) High resolution TEM lattice image of bottom part of the cross-section. (f) High resolution TEM lattice image of top part of the cross-section.

However, the grain boundaries lower the light reflectivity of the coatings because these boundary regions with disordered atom distributions results in a certain degree of light scattering and lowers the light reflectivity of coatings. The smaller the grain size, the larger the fraction of area occupied by the boundary regions, and thus the lower the light reflectivity. This optical performance is similar to the performance of the electrical properties.

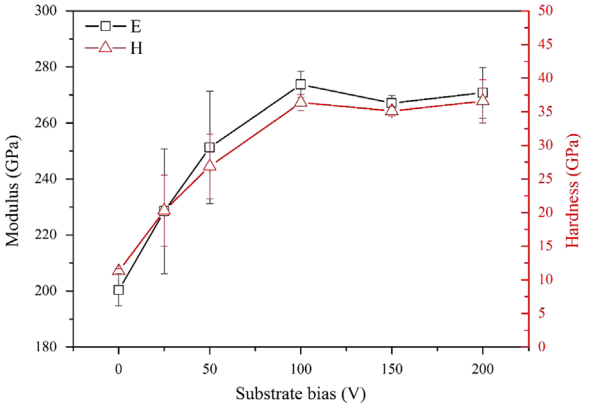

Fig. 9. Hardness and elastic modulus of the (CrTaTiVZr)N coatings deposited at different substrate biases.

Table 1
The H_{total}, H_i, ΔH_s, ΔH_g, and ΔH_v of the (CrTaTiVZr)N deposited at various substrate biases.

Substrate bias (V)	H_{total} (GPa)	H_i (GPa)	ΔH_s (GPa)	ΔH_g (GPa)	ΔH_v (GPa)
0	11.29	14.60	−0.52	7.09	−9.88
−25	20.30	14.62	2.01	10.55	−6.88
−50	26.88	14.68	2.79	14.43	−5.02
−100	36.37	14.64	4.61	17.12	0.00
−150	35.11	14.60	4.50	16.01	0.00
−200	36.57	14.67	4.41	17.49	0.00

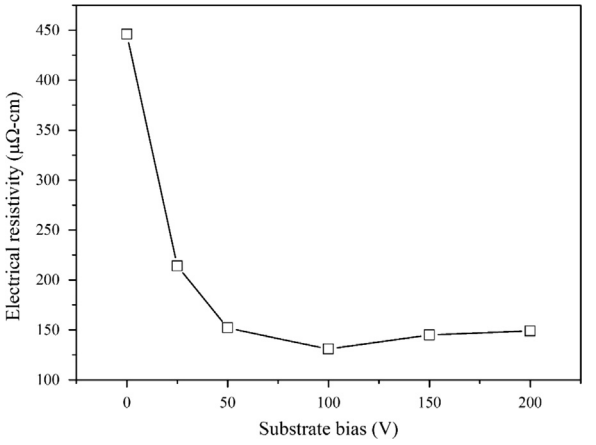

Fig. 10. Electrical resistivity of the (CrTaTiVZr)N coatings deposited at different substrate biases.

4. Discussions

4.1. Growth mechanism of (CrTaTiVZr)N coatings without substrate bias

For the (CrTaTiVZr)N coatings deposited at the substrate bias of 0 V, the structure is composed of V-shaped columns, which is typical for the zone T structure proposed by Thornton [34], as shown in Figs. 6 and 7. We can conclude that in zone T depositions, different grains with random orientation tend to nucleate at the initial growth stage. As a result of anisotropy in growth rate, which depends on the crystallographic orientation, some grains outgrow others. As the coating grows

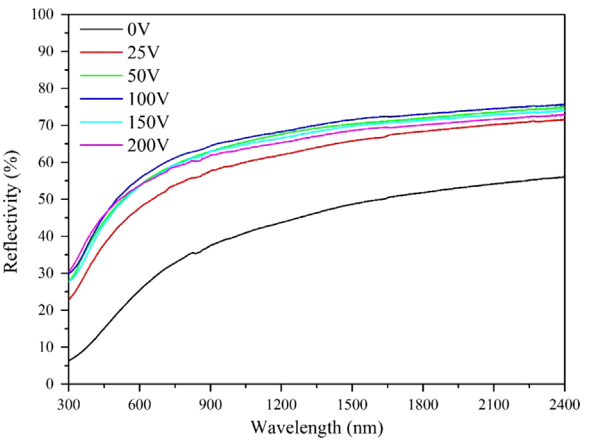

Fig. 11. Light reflectivity of the (CrTaTiVZr)N coatings deposited at different substrate biases.

further, only the grains with the highest growth rate out-of-plane planes eventually survive, resulting in V-shaped and faceted columns. This phenomenon is also known as the "evolutionary selection rule". In the case of the FCC [NaCl-type] structure, the (111) plane has the highest number of nearest interacting neighbors and thus, has the fastest growth rate [35]. As a result, the (111) out-of-plane orientation is preferred. Furthermore, numerous voids exist at the grain boundary of coatings, which is known to be generated by the lower adatom mobility and shadowing effect. Thus, the tensile stress is generated by the shrinkage of the grain boundaries mainly because of the attraction between grains at grain boundaries [36]. The observation suggests that the (CrTaTiVZr)N coatings without substrate bias do not show excellent mechanical and electrical properties because they have void boundaries with low mass density.

4.2. Effect of substrate bias on structural evolution of coating

The experimental results point to the existence of two regions for the effect of substrate bias on the structure of the (CrTaTiVZr)N coatings, which indicates that various mechanisms exist for the deposition of the (CrTaTiVZr)N coatings in the different substrate bias ranges. In the substrate bias range of 0 to −100 V, the increase of substrate bias results in five effects: (i) grain refinement, (ii) lattice expansion, (iii) (200) preferred orientation, (iv) increment of compressive stress, and (v) densification of structure. Without bias voltage, the coatings are porous. When a substrate bias is applied, the gas and metallic ions, which are accelerated by the substrates voltage, bombard the substrate. With the increase of substrate bias, the energetic ion bombardment on growing coatings becomes more intense. This finding causes coating densification by decreasing the voided regions in the microstructure by a momentum-driven displacement of the atoms. Except for the effect of void elimination, the bombardment of energetic ions strikes the surface atoms into the deeper part of the coatings and they become trapped in the layer, which is typical for the "atomic peening effect". The entrapped atoms cause lattice expansion and corresponding compressive stress [37]. Meanwhile, a series of primary and recoil collisions can

induce defects in the coating and a certain degree of renucleation may occur [38,39], indicating a reduction in the average grain size. Moreover, other possible factors, composition variation, phase separation, and internal stress must be considered. The lower nitrogen content at higher substrate bias results in more vacant N sites, thereby limiting the grain growth. Phase separation should be negligible since no other phase is observed. A large internal stress is usually accompanied by small grain size due to lattice strain. Therefore, the increased internal stress with substrate bias retards the grain growth. For the FCC [NaCl-type] structure, the (111) planes have the densest arrays of atoms, so it suffers the most from collision cascades. The (200) planes are less distorted because of their more open channeling, which means that they have the highest probability of survival. Therefore, under energetic conditions, the preferred orientation, which changes from (111) to (200), evolves.

The second region is in the substrate bias range of −100 to −200 V. In this substrate bias range, the increase of substrate bias results in the slight lattice shrinkage and stress relaxation. According to the widely accepted subplantation model [40], the high thermal energy transferred from the energetic bombardments enhances the mobility of lattice atoms in the deposited coating and forms a local "thermal spike" [41,42]. The thermal spikes are assumed to reduce the stress by adjusting the atom location or releasing implanted atoms from their metastable positions within the growing coating [41]. In summary, the effect of stress relaxation caused by the thermal spike begins to play an important role and becomes more pronounced with increasing substrate bias. This result leads to the continuous decrease of internal stress and corresponding lattice shrinkage, which is consistent with our findings. On the other hand, there is only a slight decrease in grain size with substrate bias. This may be attributed to the influence of thermal spike effect. The present study suggests that this substrate bias allows high deposition energy and a denser coating, which enhance the control of the thin coating microstructure as well as the resulting mechanical and electro-optical properties.

Despite the concern over the complexity of the material system when incorporating multiple components during its application to coatings, fortunately, the above analyses indicate the homogeneous composition and simple crystal structures of the deposited coatings. This is attributed to high mixing entropies contributed by incorporating multi-principal elements, stabilizing the existence of simple crystal structures in the form of single solid solution phase rather than compound phases. Thus, the structural evolution is what can be expected from conventional nitride coating material produced by magnetron sputtering. Based on the similar concept, the effect of the process parameters on the properties of HEA nitrides is somewhat predictable. The rapid application development of coating technology of HEA nitrides is expected.

5. Conclusion

The (CrTaTiVZr)N_x coatings prepared by reactive radio frequency magnetron sputtering at different substrate bias conditions exhibit a single NaCl-type face-centered cubic structure. The application of substrate bias results in the atomic peening and thermal spike effect. In the substrate bias range of 0 to −100 V, the atomic peening effect dominates the structural evolution of coatings, thereby causing significant lattice expansion and corresponding enhanced compressive stress. The microstructure of the coatings changes from a typical columnar structure to a dense and fine fiber structure. The large grain refinement is due to the enhanced renucleation rate by energetic bombardment-induced defects. The coating texture is transformed from (111) to (200), and is attributed to the more open channeling of (200) planes. In the substrate bias range of −100 to −200 V, the local heating thermal spike in the area of impact enhanced adatom mobility to eliminate several implanted atoms from their metastable positions within the coating, which led to slight lattice shrinkage and stress relaxation. At the substrate bias of −100 V and higher, the coatings show a high hardness value of 35−37 GPa, low electrical resistivity of 131−149 μΩ-cm, and high light reflectivity near 2000 nm of 74%. The superior physical properties of the coatings are caused by the more dense structure formed at higher substrate bias.

Acknowledgments

The authors gratefully acknowledge the financial support for this research by the Ministry of Science and Technology of Taiwan under Grant no. 103-2622-E-167-011-CC3.

References

[1] J.W. Yeh, S.K. Chen, S.J. Lin, J.Y. Gan, T.S. Chin, T.T. Shun, C.H. Tsau S.Y. Chang, Adv. Eng. Mater. 6 (2004) 299–303.
[2] J.W. Yeh, S.K. Chen, J.Y. Gan, S.J. Lin, T.S. Chin, T.T. Shun, C.H. Tsau S.Y. Chang, Metall. Mater. Trans. A 35 (2004) 2533–2536.
[3] Y. Zhang, T.T. Zuo, Z. Tang, M.C. Gao, K.A. Dahmen, P.K. Liaw, Z.P. Lu, Prog. Mater. Sci. 61 (2014) 1–93.
[4] K.H. Cheng, C.H. Lai, S.J. Lin, J.W. Yeh, Ann. Chim. Sci. Mater. 31 (2006) 723–736.
[5] V. Braic, M. Balaceanu, M. Braic, A. Vladescu, S. Panseri, A. Russob J. Mech. Behav. Biomed. Mater. 10 (2012) 197–205.
[6] S.Y. Chang, S.Y. Lin, Y.C. Huang, C.L. Wu, Surf. Coat. Technol. 204 (2010) 3307–3314.
[7] D.C. Tsai, Z.C. Chang, B.H. Kuo, M.H. Shiao, S.Y. Chang, F.S. Shieu, Appl. Surf. Sci. 282 (2013) 789–797.
[8] D.C. Tsai, Z.C. Chang, B.H. Kuo, S.Y. Chang, F.S. Shieu, J. Alloy. Compd. 616 (2014) 646–651.
[9] Z.C. Chang, S.C. Liang, S. Han, Y.K. Chen, F.S. Shieu, Nucl. Instrum. Methods Phys. Res. Sect. B 333 (2014) 1–5.
[10] D.C. Tsai, Z.C. Chang, B.H. Kuo, T.N. Lin, M.H. Shiao, F.S. Shieu, Surf. Coat. Technol. 240 (2014) 160–166.
[11] H.T. Hsueh, W.J. Shen, M.H. Tsai, J.W. Yeh, Surf. Coat. Technol. 206 (2012) 4106–4112.
[12] M.H. Tsai, C.H. Lai, J.W. Yeh, J.Y. Gan, J. Phys. D: Appl. Phys. 41 (2008) 235402.
[13] H.E. Cheng, W.J. Lee, M. Hsu, Thin Solid Films 485 (2005) 59–65.
[14] H.C. Chung, C.P. Liu, Surf. Coat. Technol. 200 (2006) 3122–3126.
[15] J.L. Ruan, D.F. Lii, J.S. Chen, J.L. Huang, Ceram. Int. 35 (2009) 1999–2005.
[16] G. Duan, G. Zhao, L. Wu, X. Lin, G. Han, Appl. Surf. Sci. 257 (2011) 2428–2431.
[17] S. Schleussner, T. Kubart, T. Törndahl, M. Edoff, Thin Solid Films 517 (2009) 5548–5552.
[18] J.K. Park, Y.J. Baik, Mater. Lett. 62 (2008) 2528–2530.
[19] S.H. Shin, M.W. Kim, M.C. Kang, K.H. Kim, D.H. Kwon, J.S. Kim, Surf. Coat. Technol. 202 (2008) 5613–5616.
[20] C.H. Ma, J.H. Huang, H. Chen, Thin Solid Films 418 (2002) 73–78.
[21] H.P. Klug, L.E. Alexander, X-ray Diffraction Procedures for Polycrystalline and Amorphous Materials, Wiley, New York, 1974.

[22] W.J. Shen, M.H. Tsai, Y.S. Chang, J.W. Yeh, Thin Solid Films 520 (2012) 6183–6188.
[23] U.C. Oh, J.H. Je, J. Appl. Phys. 74 (1993) 1692–1696.
[24] N.H. Hoang, D.R. McKenzie, W.D. McFall, Y. Yin, J. Appl. Phys. 80 (1996) 6279–6285.
[25] D.R. McKenzie, Y. Yin, W.D. McFall, N.H. Hoang, J. Phys.: Condens. Matter 8 (1996) 5883–5890.
[26] M.K. Lee, H.S. Kang, W.W. Kim, J.S. Kim, W.J. Lee, J. Mater. Res. 12 (1997) 2393–2400.
[27] M. Kobayashi, Y. Doi, Thin Solid Films 54 (1984) 67–74.
[28] P. Patsalas, C. Charitidis, L. Logothetidis, Surf. Coat. Technol. 125 (2000) 335–340.
[29] S. Khan, M. Mehmood, I. Ahmad, F. Ali, A. Shah, Mater. Sci. Semicond. Process. 30 (2015) 486–493.
[30] C. Lu, Y.W. Mai, Y.G. Shen, J. Mater. Sci. 41 (2006) 937–950.
[31] G. Frank, E. Kauer, H. Kostlin, Thin Solid Films 77 (1981) 107–118.
[32] D.C. Tsai, Z.C. Chang, B.H. Kuo, C.T. Tsao, E.C. Chen, F.S. Shieu, J. Alloy. Compd. 622 (2015) 446–457.
[33] Y.H. Kim, J.K. Park, D.K. Lim, H.B. Kang, Light-transmissive polycrystalline alumina ceramics, U.S. Pat. 5376, 606 (1994).
[34] J.A. Thornton, J. Vac. Sci. Technol. A 4 (1996) 3059–3065.
[35] G. Abadias, Y.Y. Tse, P. Guérin, V. Pelosin, J. Appl. Phys. 99 (2006) 113519.
[36] F.A. Doljack, R.W. Hoffman, Thin Solid Films 12 (1974) 71–74.
[37] M. Kobayashi, T. Matsui, Y. Murakami, Int. J. Fatigue 20 (1998) 351–357.
[38] G. Håkansson, J.-E. Sundgren, D. McIntyre, J.E. Greene, W.-D. Münz, Thin Solid Films 153 (1987) 55–65.
[39] L. Zhang, G. Ma, H. Ma, G. Lin, Nucl. Instrum. Methods Phys. Res. Sect. B 333 (2014) 1–5.
[40] D.V. Shtansky, Y.Y. Takamura, T. Yoshida, Y. Ikuhara, Sci. Technol. Adv. Mater. 1 (2000) 219–225.
[41] M.M.M. Bilek, D.R. McKenzie, R.N. Tarrant, S.H.M. Lim D.G. McCulloch, Surf. Coat. Technol. 156 (2002) 136–142.
[42] N.A. Marks, Phys. Rev. B 56 (1997) 2441–2446.